

2013

Fundamental Limits of Detection in the Near and Mid Infrared

Nathan Lenssen
Claremont McKenna College

Recommended Citation

Lenssen, Nathan, "Fundamental Limits of Detection in the Near and Mid Infrared" (2013). *CMC Senior Theses*. Paper 800.
http://scholarship.claremont.edu/cmc_theses/800

This Open Access Senior Thesis is brought to you by Scholarship@Claremont. It has been accepted for inclusion in this collection by an authorized administrator. For more information, please contact scholarship@cuc.claremont.edu.

Fundamental Limits of Detection of Galaxies in the Near and Mid Infrared

Senior Thesis in Physics

Nathan Lenssen

Claremont McKenna College

Dr. Philip Lubin

University of California, Santa Barbara

Dr. James Higdon

Keck Science Department

Table of Contents

1. Abstract.....	2
2. Introduction	2
3. Infrared Missions	3
3.1 Ground Based.....	3
3.1.1 W. M. Keck Observatory	3
3.1.2 Gemini.....	4
3.1.3 Stratospheric Observatory for Infrared Astronomy.....	4
3.2 Extra-Terrestrial	4
3.2.1 Spitzer Space Telescope.....	4
3.2.2 James Webb Space Telescope	4
3.3 Modeled Telescopes	4
4. Noise	5
4.0.1 Units.....	6
4.0.2 Background Limiting Noise Generated (BLING).....	7
4.0.3 The Black Body.....	9
4.1 Emissivity of Telescope	10
4.1.1 Bulk Emissivity Model	10
4.1.2 Application of Emissivity Model.....	11
4.2 Cosmic Microwave Background.....	13
4.3 Cosmic Infrared Background.....	15
4.4 Zodiacal Emission.....	18
4.5 Other Atmospheric Effects.....	21
4.6 Interpolation	22
4.7 Total Noise Calculation	23
5. Signal.....	24
5.1 SED Data.....	24
5.2 Dusty Galaxy SED Model (Denny et al. 2013)	25
5.3 Signal Integration	30
6. Integration Time.....	30
6.1 Limiting Signal	32
7. Conclusions	33
8. Acknowledgements.....	34
9. References	35

1. Abstract

The construction of the James Webb Space Telescope has brought attention to infrared astronomy and cosmology. The potential information about our universe to be gained by this mission and future infrared telescopes is staggering, but infrared observation faces many obstacles. These telescopes face large amounts of noise by many phenomena, from emission off of the mirrors to the cosmic infrared background. Infrared telescopes need to be designed in such a way that noise is minimized to achieve sufficient signal to noise ratio on high redshift objects. We will investigate current and planned space and ground based telescopes, model the noise they encounter, and discover their limitations. The ultimate of our investigation is to compare the sensitivity of these missions in the near and mid IR and to propose new missions.

Our investigation is broken down into four major sections: current missions, noise, signal, and proposed missions. In the proposed missions section we investigate historical and current infrared telescopes with attention given to their location and properties. The noise section discusses the noise that an infrared telescope will encounter and set the background limit. The signal section will look at the spectral energy distributions (SED) of a few significant objects in our universe. We will calculate the intensity of the objects at various points on Earth and in orbit. In the final section we use our findings in the signal and noise sections to model integration times (observation time) for a variety of missions to achieve a given signal to noise ratio (SNR).

2. Introduction

One of the more challenging regions of the electromagnetic spectrum to observe in is the near and mid infrared. Difficulty arises from the large quantities of noise generated by the telescope and the matter the telescope is looking through. When considering telescopes located within the atmosphere, we also need to account for the absorption and emission created by our atmosphere while for space the cost and feasibility of orbital missions become major concerns. Cosmology currently has many questions and proposed theories that would benefit from high sensitivity observations in this part of the spectrum. Examples of such phenomenon are the search for first light and the search for planets in other solar systems (Gardener et al. 2006)(National Research Council 2010).

Our study can be viewed as a synthesis of numerous infrared models for the noise and signal that an infrared telescope encounters from 0.2-30 microns. Signal refers to light that comes from an object of interest which in this paper will be a distant galaxy with a spectrum running from ultraviolet radiation through microwave or approximately 10nm to 1mm. Distant galaxies are but one class of objects of interest in the IR. Noise is a term that accounts for all other light hitting our detector. We will also investigate how we can model a galaxy emitting in the infrared as well as what we can do to minimize noise. With information on the spectra of light our infrared telescope will be used to analyze and compare several possible observation missions.

In section 3, we present a brief summary of a few current and past infrared telescopes. By learning about some major ground and space based telescopes, we gain an understanding of the current

strategies of observation. We will provide a baseline and context for the eventual missions we will simulate with our models.

In section 4, we investigate the noise that our telescopes will encounter. By modeling backgrounds that are bright in the near and mid infrared, we gain an understanding of the origins of stray light coming from space, as well as their absolute magnitudes. We also investigate noise created within our atmosphere and discuss how the altitude of our telescope can affect noise levels.

In section 5, we create models for sample galaxies. We model the spectral energy distribution (SED) of a galaxy and account for the absorption the light encounters as it travels to the telescope to determine how much light we will see.

In section 6, we combine sections 4 and 5 by proposing mission scenarios and calculating integration times based off of our signal and noise spectra. We will compare these scenarios and comment on the advantages and disadvantages of each.

3. Infrared Missions

A key part of our study is to understand what methods have been used to collect infrared observations in the past. In researching other missions we gain knowledge of what methods scientists have used in the past as well as the advantages and disadvantages of their methods. For each mission we will take note of a few key parameters. The mirror temperature and emissivity will be useful for analysis of the noise generated by the emission of light off of the telescope. The size of the primary mirror and the telescope's field of view will facilitate comparison of the telescopes' respective ability to perform tasks ranging from wide scale surveys to ultra deep images. The location of the telescope will be crucial in determining what background emissions and absorptions occur. In the next section we will break down the telescopes by both their operational status and whether they are located on or near the ground or in space.

3.1 Ground Based

3.1.1 W. M. Keck Observatory

Until the construction of the 10.4 m diameter Gran Telescopio Canarias in the Canary Islands in 2009, the twin 10m telescopes, Keck I and Keck II, near the summit of Mauna Kea in Hawaii were the largest in the world. Such large diameters on the mirror are enabled by using a segmented design with aluminum-coated glass hexagonal segments. Located at an altitude of 4,145m, the Keck telescopes are able to reduce the impact the atmosphere has on incoming light. The telescopes have many instruments some of which are sensitive in the near infrared and are of interest in this study. The second Near Infrared Camera (NIRC-2) is a super high resolution camera and spectroscope that operates from 1 to 5 microns (Goodrich, 2002). NIRC-2 is unique because it uses the adaptive optics on Keck II in which corrects signals that are warped in the atmosphere. Keck contains the near infrared spectrograph (NIRSPEC) which is a cryogenic high-resolution spectrograph with a waveband of 0.95 to 5.4 microns that boasts an impressive resolving power $R \sim 25,000$.

Keck serves as a good benchmark for a large land based telescope. While not specifically designed as an IR telescope and severely hampered by both warm optics and a significant amount of atmosphere it is still relevant in our discussion as a ground based telescope. (See <http://keckobservatory.org/> and <http://www.gtc.iac.es/en/> for more information)

3.1.2 Gemini

The Gemini telescopes are twin 8.1m with one located in Chile at over 2,700m and the other located on Mauna Kea near Keck. Gemini is very comparable to Keck in many respects, but it sets itself apart with its silver mirror coating. Silver has a significantly higher reflectivity (and thus lower emissivity) than the aluminum in Keck, which reduces the amount of noise off of the warm mirrors. In our study we will use the Gemini telescopes as an example of a large, ground based telescope with a silver coated mirror at high altitude.

3.1.3 Stratospheric Observatory for Infrared Astronomy

While not located on the ground, the Stratospheric Observatory for Infrared Astronomy's (SOFIA) 13.7km altitude of operation qualifies closer to a ground based telescope as it still encounters most of the disadvantages a telescope on Mauna Kea does due to the atmosphere. SOFIA has a 2.5m aluminum mirror located near the tail of a modified 747 which gives it the unique ability to move rapidly around the world to chase time sensitive objects. In this study SOFIA will primarily be compared with a balloon telescope which can reach altitudes of 40km and cost a fraction of the price.

3.2 Extra-Terrestrial

3.2.1 Spitzer Space Telescope

The Spitzer Space Telescope launched in 2003 and operated until it ran out of cryonic material in 2009. The telescope used a 0.85m primary mirror composed of polished beryllium that was cooled to 5.5K. The low mirror temperature allowed Spitzer to be limited by the zodiacal emission rather than its optics. Beryllium was chosen for its high stiffness to density ratio which provides light mirrors that hold shape as they cool. Spitzer observed from the mid infrared into the far infrared with instrumentation from 3.6-160 microns (Werner et al. 2004).

3.2.2 James Webb Space Telescope

One of the major sources of inspiration and data for this investigation is the James Webb Space Telescope (JWST). JWST is currently under development by NASA and is aiming for a 2018 launch (www.jwst.nasa.gov). With a waveband of 0.6-29 microns, cooled optics, and high sensitivity cameras and spectrometers, JWST will serve as a benchmark for this study. JWST will have a segmented 6.5m gold-coated primary mirror that will be radiatively cooled to under 50 K. It will observe from orbit around the Sun-Earth Lagrange point L2 where it will be above the infrared noise in the Earth's atmosphere. A drawback to this mission is the cost which is currently close to \$10 billion (Cowen).

3.3 Modeled Telescopes

In this study we analyze the quantity of noise and strength of signal that a range of telescopes will encounter. See table below for the parameters used in our model. For Keck, SOFIA, and JWST we used as accurate data as possible within the confines of our model. For Keck it must be noted that Keck is not

optimized for infrared observation. For this study we assume a Keck-like telescope located at the same position that has been IR optimized. Our calculations regarding SOFIA use our emissivity model outlined in section 4.1. These modeled numbers fall far below the 15-25% emissivities reported by various SOFIA teams. We are using a very low value here for a potential future SOFIA like telescope. For the balloon telescope we decided to use parameters that are futuristic in terms of diameter and temperature. For a high altitude telescope it might be possible to run the mirror just above the liquefaction point of the atmosphere. We note that the emissivity is a critical issue for IR telescopes and a high emissivity will severely hamper its performance. The specific design of the telescope is also critical and many visible light telescopes are used in the IR (such as Keck) and suffer from significant excess emissivity that an optimized IR specific telescope would not.

Telescope	Keck	SOFIA	Balloon	JWST
Altitude (km)	4	12.5 (12-13.7)	40	N/A
Mirror Temperature (K)	270	230	100	50
Mirror Diameter (m)	10	2.5	10	6.5
Mirror Coating	Aluminum	Aluminum	Aluminum	Gold

4. Noise

The final result we are aiming for are the integration times for certain telescope setups pointing at a variety of galaxies. Integration time is the amount of time a telescope needs to look at a source such as a galaxy before it has detected a statistically significant quantity of photons. These times are calculated through the ratio between signal and noise – this is referred to as the SNR or Signal to Noise Ratio. The signal is the number of photons from the target galaxy that hit the detector of the telescope in a given time while the noise is the statistical fluctuations of the total number of photons that hit the detector. The noise term includes all photons including those from the source. This section will discuss what the significant sources of noise in the near and mid infrared. We will investigate three categories of noise: noise generated by the telescope, noise generated within our atmosphere, and noise generated by the many backgrounds in space as well as the noise (or photon statistics) from the source itself. For each of these cases we will discuss the cause of the light, how much of a problem it is for our observations, and how the impact of this noise on our study can be reduced.

4.0.1 Units

Throughout this paper we will use units that may be unfamiliar to the reader. When we describe quantities of light, our most general unit is spectral radiance. In the study our core units of spectral radiance are named I and are

$$I(\lambda) = \frac{W}{m^2 \cdot \text{arc sec}^2 \cdot \mu\text{m}} \quad (4.1)$$

$$I(\nu) = \frac{W}{m^2 \cdot \text{arc sec}^2 \cdot \text{Hz}} \quad (4.2)$$

Here the W describes the amount of power (watts), m^{-2} represents the telescope's mirror, arc sec^{-2} represents the solid angle of the sky that the telescope views, and μm^{-1} and Hz^{-1} are used since we will have data of either per wavelength or frequency.

Many of the radiances we encounter have very small values of energy. In these cases it is more intuitive to think about the flux of individual photons rather than the energy of these photons. For a photon

$$E = \frac{hc}{\lambda} = h\nu \quad (4.3)$$

Dividing by this relationship with our $I(\lambda)$ and $I(\nu)$ values from above allows for two new units that we will name N

$$N(\lambda) = I(\lambda) \cdot \frac{\lambda}{hc} = \frac{\text{Photons}}{\text{sec} \cdot m^2 \cdot \text{arc sec}^2 \cdot \mu\text{m}} \quad (4.4)$$

$$N(\nu) = I(\nu) \cdot \frac{1}{h\nu} = \frac{\text{Photons}}{\text{sec} \cdot m^2 \cdot \text{arc sec}^2 \cdot \text{Hz}} \quad (4.5)$$

For more intuitive units we will also sometimes integrate out the area and solid angle from our N units to be able to work in just spectral photons per second. The integration of area and solid angle is equivalent to multiplying by the Area of the mirror A and by the solid angle on the sky per pixel Ω . For a diffraction limited system this integral conveniently reduces to $A \cdot \Omega = \lambda^2 = \frac{c^2}{\nu^2}$

$$P(\lambda) = N(\nu) \cdot A \cdot \Omega = \frac{\text{Photons}}{\text{sec} \cdot \mu\text{m}} \quad (4.6)$$

We also must make note of the conversion from μm^{-1} to Hz^{-1} . All of our equations in this section so far are fluxes and can be viewed mathematically as differential equations. Thus when trying to convert from $N(\lambda)$ to $N(\nu)$ we have

$$N(\lambda)d\lambda = N(\nu)d\nu \quad (4.7)$$

$$N(\lambda) = N(\nu) \frac{d\nu}{d\lambda}$$

But we have the relationship between ν and λ is simply $\nu = c/\lambda$ so

$$\frac{d\nu}{d\lambda} = \frac{d}{d\lambda} \frac{1}{\lambda} = -\frac{1}{\lambda^2} \quad (4.8)$$

We drop the negative sign as it does not make physical sense and has no impact on the overall math and are left with the conversion

$$N(\lambda) = N(\nu) \frac{1}{\lambda^2} \quad (4.9)$$

In this same way we can convert from flux per wavelength to flux per frequency.

The physical intuitiveness of counting photons that the N and P units offer is useful in grasping the meaning of numbers in this study. We gain understanding of the very small levels of light that is effectively emitted by our source as well as the low tolerance for noise in our system.

In this study we will also deal with two different units for the solid angle of the sky that our telescope is viewing since cosmologists and astronomers move between square arc seconds (arcsec^2) and steradians (sr). The conversion between the two is a two-dimensional analogue to the conversion between degrees and radians when discussing angle.

A common unit used when describing small fluxes originating from small points in space is the Jansky (Jy). One Jansky is simply defined as

$$1 \text{ Jy} = 10^{-26} \frac{W}{m^2 \text{ sr Hz}} \quad (4.10)$$

4.0.2 Background Limiting Noise Generated (BLING)

The choice of $N(\lambda)$ and $P(\lambda)$ provide intuitive ways to look at the noise our systems will encounter. Unfortunately these units contain differential terms in area and solid angle that our signal will not have. Thus we need to find a way to transform our noise into a format that can be used in signal to noise calculations. Detector performance is often specified by noise equivalent power (NEP) which is the signal that provides a signal to noise ratio of 1. Another useful unit commonly used is the background limited performance (BLIP). NEP, BLIP and BLING have units of $\frac{W}{\sqrt{Hz}}$ and can easily be related to our signal. Our study is aimed at modeling integration times and to facilitate such calculations we aim to define our system noise in terms of the background limited noise generated (BLING). We define BLING as

$$\zeta = P_N t^{\frac{1}{2}} \quad (4.11)$$

With noise power P_N and integration time t . Unfortunately the calculation of BLING from the quantities we currently possess is not as simple as equation 4.11 would indicate. First we define the power per unit bandwidth for a system as

$$S(\nu) = I(\nu)A\Omega \quad (4.12)$$

Where $I(\nu)$ is as defined previously, A is the collection area, and Ω is the solid angle that a telescope views on the sky. In this study, we assume that our optics are diffraction limited which allows us to use the relationship

$$A\Omega = \lambda^2 = \frac{c^2}{\nu^2} \quad (4.13)$$

Combining with equation 4.12 yields

$$S(\nu) = \frac{I(\nu)c^2}{\nu^2} \quad [W] \quad (4.14)$$

With our power per unit bandwidth defined in terms of quantities we understand, we can now calculate the total power P around ν_0 with bandwidth $\Delta\nu$ by integrating our equation for $S(\nu)$

$$P(\nu_0, \Delta\nu) = 2 \int_{\nu_0 - \frac{\Delta\nu}{2}}^{\nu_0 + \frac{\Delta\nu}{2}} S(\nu) d\nu \quad [W] \quad (4.15)$$

Recalling that the energy of a photon can be described by $E_{photon} = h\nu$ we calculate the number of photons with a specific energy as

$$N(\nu_0, \Delta\nu) = \frac{P(\nu_0, \Delta\nu)}{E_{photon}(\nu_0, \Delta\nu)} = \int_{\nu_0 - \frac{\Delta\nu}{2}}^{\nu_0 + \frac{\Delta\nu}{2}} \frac{S(\nu)}{h\nu} d\nu \quad \left[\frac{Photons}{s} \right] \quad (4.16)$$

To calculate the total number of photons that we collect in a specific integration time t we simply multiply our rate by our integration time. Thus the mean number of photons collected is

$$\bar{N}(\nu_0, \Delta\nu) = N(\nu_0, \Delta\nu)t \quad (4.17)$$

Since the BLING is essentially the uncertainty of the number of photons collected multiplied by the energy of the photons we need to calculate the uncertainty. This is done by

$$\delta N(\nu_0) = N(\nu_0)^{\frac{1}{2}} = (N(\nu_0) \cdot t)^{\frac{1}{2}} = \left(t \cdot \int_{\nu_0 - \frac{\Delta\nu}{2}}^{\nu_0 + \frac{\Delta\nu}{2}} \frac{S(\nu)}{h\nu} d\nu \right)^{\frac{1}{2}} \quad (4.18)$$

It is important to note that the statistical fluctuation in the number of photons has two terms. Photons are bosons (integral spin) since the spin of a photon is 1. The two terms are given by $\delta N(\nu_0) = [N(\nu_0) + N(\nu_0)^2]^{\frac{1}{2}}$ However this only applies for completely correlated sources of photons. Our sources are essentially all uncorrelated not only from each other but within the source itself. The second

term is effectively a collective coherent term that would be relevant if we were observing coherent sources such as a laser but we are not. All of our physical processes are from random uncorrelated processes. In our calculation of BLING we will calculate the uncertainty each second so we set $t=1$. Thus our expression for BLING is

$$\zeta(\nu_0) = E_{photon} \delta\mathcal{N}(\nu_0) = \left(\int_{\nu_0 - \frac{\Delta\nu}{2}}^{\nu_0 + \frac{\Delta\nu}{2}} h\nu S(\nu) d\nu \right)^{\frac{1}{2}} \left[\frac{W}{\sqrt{Hz}} \right] \quad (4.19)$$

In cosmology we are usually provided with a spectral resolution R instead of a bandwidth so we make the substitution $R = \frac{\nu}{\Delta\nu}$

$$\zeta(\nu_0) = \left(\int_{\nu_0 - \frac{\Delta\nu}{2R}}^{\nu_0 + \frac{\Delta\nu}{2R}} h\nu S(\nu) d\nu \right)^{\frac{1}{2}} \left[\frac{W}{\sqrt{Hz}} \right] \quad (4.20)$$

4.0.3 The Black Body

Essentially all of the light we investigate in this study can be modeled by a black body or some linear combination of black bodies. A black body is an idealized radiator at constant temperature whose radiation spectrum is defined by Planck's law. In terms of a frequency λ , the spectral radiance $I(\lambda, T)_{bb}$ at temperature T is

$$I(\lambda, T)_{bb} = \frac{2hc^2}{\lambda^5} \frac{1}{e^{\frac{hc}{\lambda k_B T}} - 1} \left[\frac{W}{m^2 \cdot sr \cdot micron} \right] \quad (4.21)$$

To convert from $I(\lambda, T)_{bb}$ to $N(\lambda, T)_{bb}$ we divide by the energy of a photon (hc/λ) as shown in section 4.0.1 yielding

$$N(\lambda, T)_{bb} = \frac{2c}{\lambda^4} \frac{1}{e^{\frac{hc}{\lambda k_B T}} - 1} \left[\frac{photons}{m^2 \cdot s \cdot sr \cdot micron} \right] \quad (4.22)$$

We also are sometimes interested in knowing the raw output of the source in photons per second. To calculate these values we integrate $N(\lambda, T)_{bb}$ over the area of the detector and the solid angle of the detector acceptance. This is equivalent to multiplying by the Area of the mirror A and by the solid angle on the sky per pixel Ω . For a diffraction limited system this integral conveniently reduces to $A \cdot \Omega = \lambda^2$ yielding

$$P(\lambda, T)_{bb} = \frac{2c}{\lambda^2} \frac{1}{e^{\frac{hc}{\lambda k_B T}} - 1} \left[\frac{photons}{s \cdot micron} \right] \quad (4.23)$$

The first application of black bodies that we encounter is in the emissivity of the mirrors in our telescopes. A major consideration in the design of any telescope is the noise generated directly by the

mirrors. An ideal mirror reflects 100 percent of incoming light providing exactly the information that it sees in the sky. In reality some of the light energy striking the mirror is absorbed and emitted in a modified black body spectrum known as a grey body. Thus the detector sees some photons that are released by the telescope. We will see that this source of noise is dependent of the temperature and composition of the mirror.

The proportion of light that is reflected is the reflectivity (R) of the mirror. The remainder of the light is absorbed and is referred to as the emissivity (ε) of the mirror. Since these two quantities are proportions for normal optical systems

$$R + \varepsilon = 1 \quad (4.24)$$

The spectrum of a grey body is simply a black body scaled by an emissivity function that is often wavelength dependent

$$I(\lambda, T)_{gb} = \varepsilon(\lambda) \frac{2hc^2}{\lambda^5} \frac{1}{e^{\frac{hc}{\lambda k_B T}} - 1} \left[\frac{W}{m^2 \cdot sr \cdot micron} \right] \quad (4.25)$$

For our $N(\lambda, T)_{bb}$ and $P(\lambda, T)_{gb}$ distribution all that is necessary is a scaling by an emissivity function as above

$$P(\lambda, T)_{gb} = \varepsilon(\lambda) \frac{2c}{\lambda^2} \frac{1}{e^{\frac{hc}{\lambda k_B T}} - 1} \left[\frac{photons}{s \cdot micron} \right] \quad (4.26)$$

We now have a qualitative understanding of the role emissivity plays in calculating the noise in a telescope system as well as a quantitative view of the general spectrum of a blackbody.

4.1 Emissivity of Telescope

4.1.1 Bulk Emissivity Model

When deciding how to model the emissivity of the telescope mirrors it was clear from experimentally determined emissivities that a constant emissivity with respect to wavelength would omit a lot of information. The Hagen-Rubens formula is useful in approximating a wavelength dependent emissivity function (Xu et al. 1996)

$$\varepsilon = \left(\frac{16\pi c \epsilon_0}{\lambda \sigma} \right)^{\frac{1}{2}} \quad (4.27)$$

Where λ is wavelength, c is the speed of light ϵ_0 is the permittivity of free space, and σ is the surface electrical conductivity of the material. The systems we compared to the model had mirrors coated in beryllium, aluminum, silver or gold and the respective surface electrical conductivities are as follows.

Material	$\sigma (\Omega^{-1} \text{ m}^{-1})$
Beryllium (Be)	$2.500 \cdot 10^7$
Aluminum (Al)	$3.538 \cdot 10^7$
Gold (Au)	$4.060 \cdot 10^7$
Silver (Ag)	$6.287 \cdot 10^7$

Source: Eddy Current Technology 1984

With the Hagen-Rubens formula and the surface electrical conductivities for the mirror materials we are able to plot our four modeled emissivity curves against a range of wavelengths. To qualitatively check how well the models work we compare researched measured emissivity measurements from a variety of telescopes and compare it to the ideal model from above.

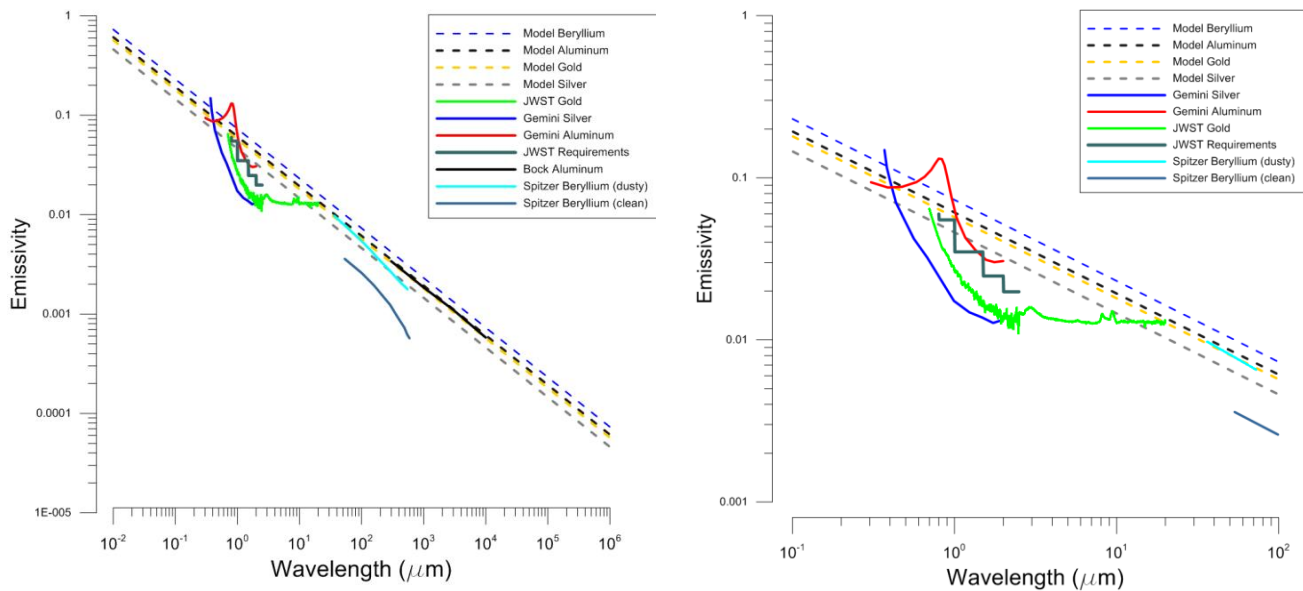


Figure 4.1: Recorded and modeled emissivities compared over two wavebands.

Sources: Gemini Observatory 2003, Lightsey 2012, Bock 1995

As it can be observed in Figure 4.1 the model does not quite match the measured values. However it provides a reasonable estimate, as the modeled values remain within an order of magnitude throughout the waveband of this investigation. Therefore, we use the Hagen-Rubens formula to model mirror emissivity due to its reasonable accuracy as well as its simplicity to compute.

4.1.2 Application of Emissivity Model

Since mirrors with non-zero emissivity act as a grey body, the spectrum and magnitude of noise they emit is highly dependent on temperature. A grey body is just a linear transformation of a black body so all of the mathematical properties of black bodies still apply. We focus on the Stefan-Boltzmann law and Wien's displacement law as they are both temperature dependent and relevant to our noise analysis.

The Stefan-Boltzmann law describes the total energy emitted per surface area per time. The black body emissive power j^* is directly proportional to Temperature raised to the fourth power

$$j^*(T) = \frac{2\pi^5 k^4}{15c^2 h^3} \cdot T^4 \quad \left[\frac{W}{m^2} \right] \quad (4.28)$$

It is shown in equation 4.28 that temperature is certainly important in keeping the amount of noise generated low. Wien's displacement law shows the wavelength at which the Planck distribution's peak occurs and it is inversely proportional to the temperature of the black body

$$\lambda_{max} \cdot T = b \quad (4.29)$$

Where T is the temperature in Kelvin, λ_{max} is the wavelength with the peak emission, and b is a constant of proportionality equal to $2.897 \cdot 10^{-3} m \cdot K$.

With total power directly proportional to wavelength and peak power inversely proportional it can be seen why lower mirror temperature are optimal for infrared telescopes. As further shown in figures 4.2 and 4.3, the black body spectrum shrinks and moves to high wavelengths rapidly.

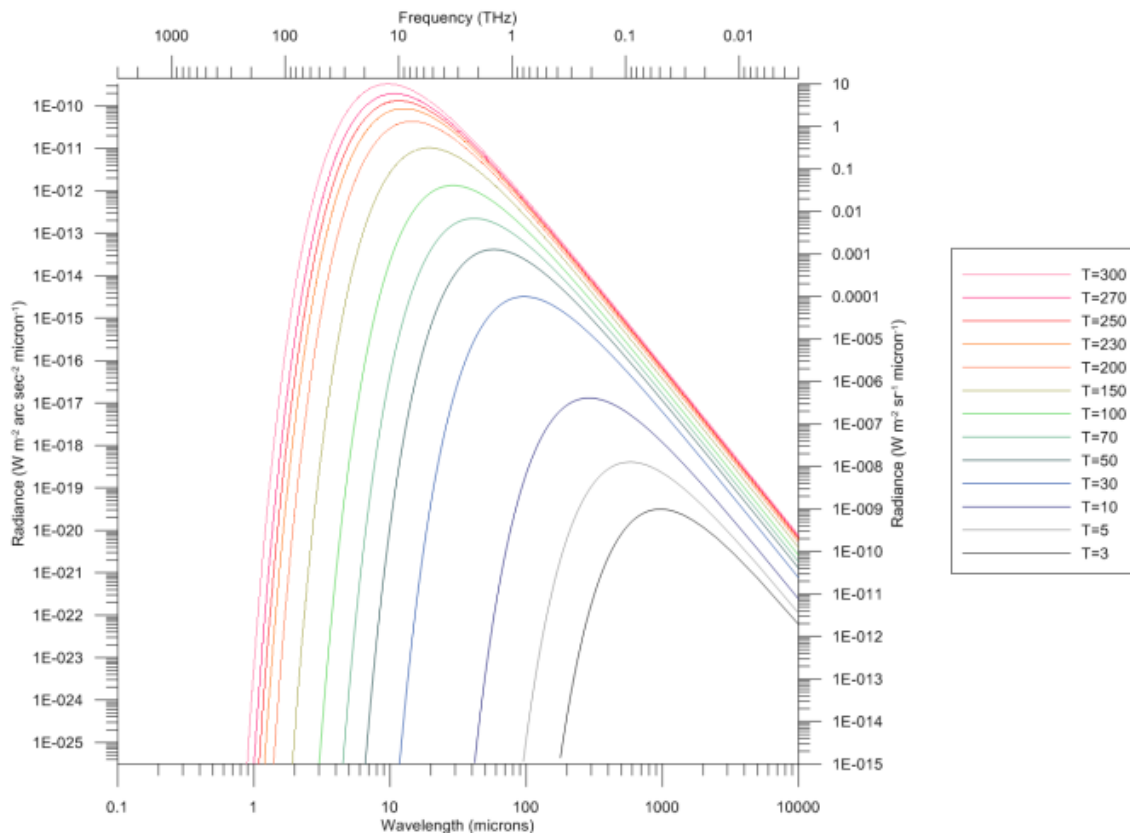


Figure 4.2: Black body emission at various temperatures

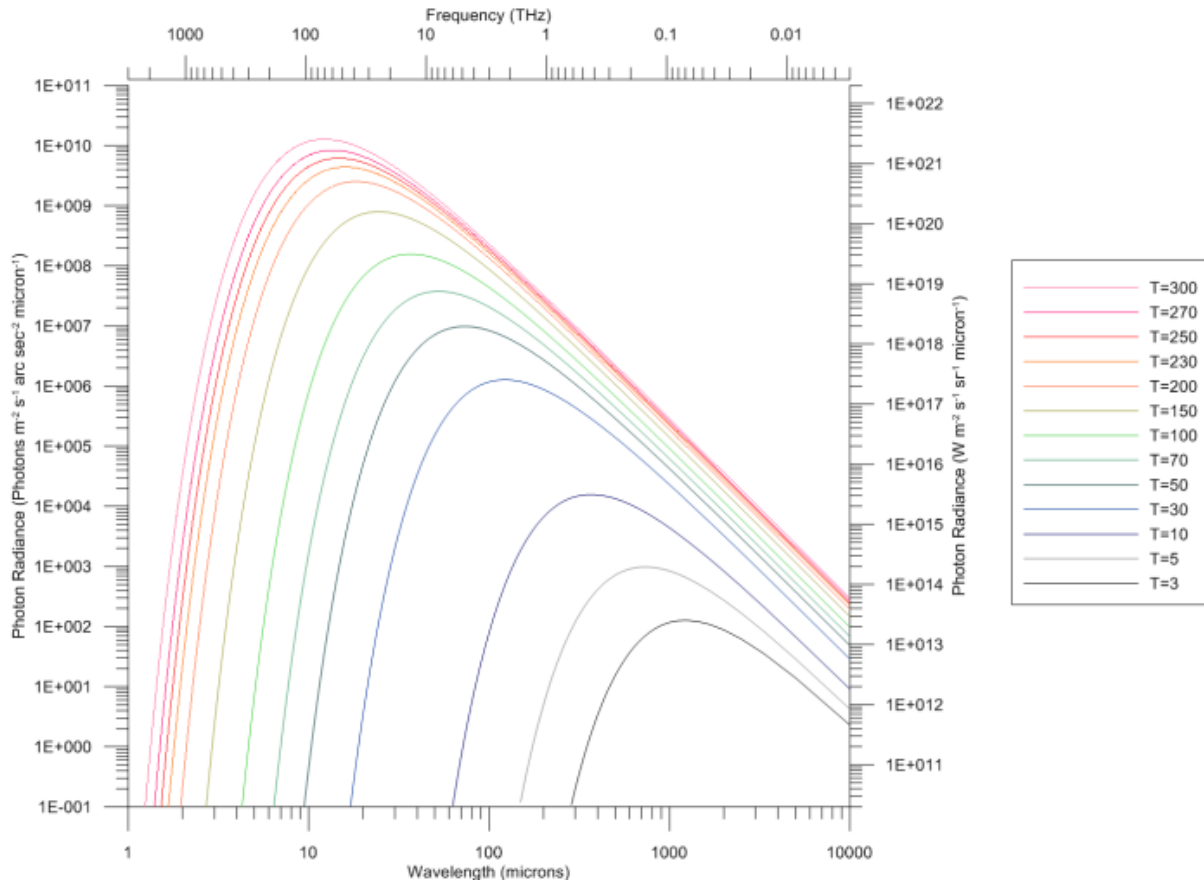


Figure 4.3: Black body photon emission at various temperatures

4.2 Cosmic Microwave Background

The most prolific background in our universe is the cosmic microwave background (CMB). Up until 300,000 years after the big bang, matter in the universe existed as a plasma of photons and electrons. These charged particles absorbed or scattered all photons inhibiting the propagation of photons through the universe. At around 300,000 years after the big bang the universe became cool enough for the protons and neutrons to combine into hydrogen atoms. Shortly after, photons were able to move freely without being scattered. These photons still exist and are distributed relatively uniformly throughout the universe. Due to the expansion of space, the waves of these photons have been stretched out over the billions of years to their present low energy state in the microwave spectrum (Planck collaboration 2005).

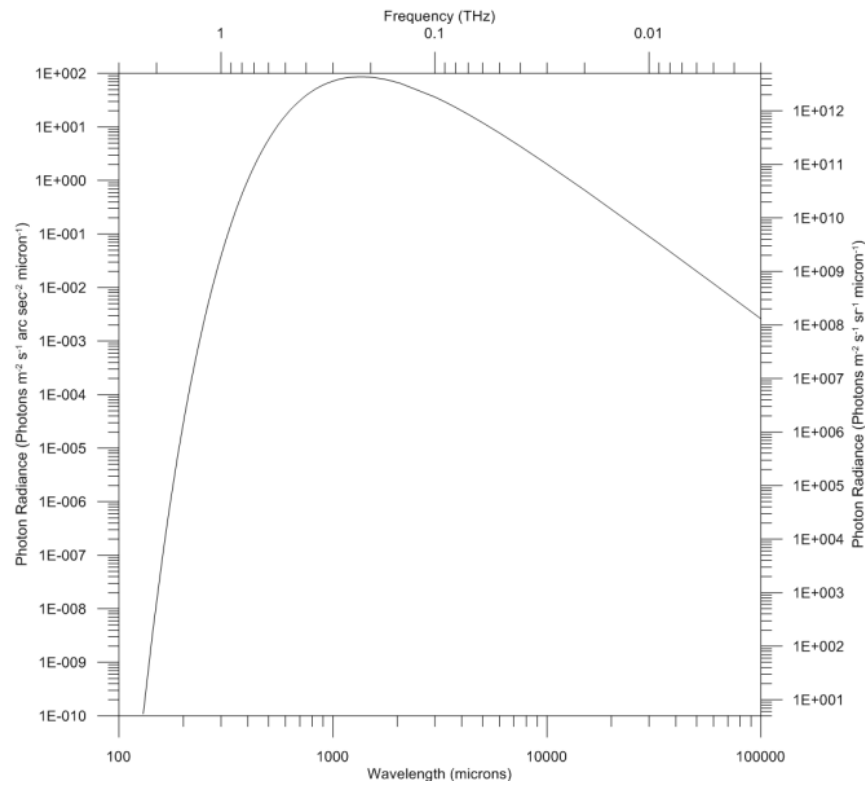


Figure 4.4: The photon emission of the cosmic microwave background

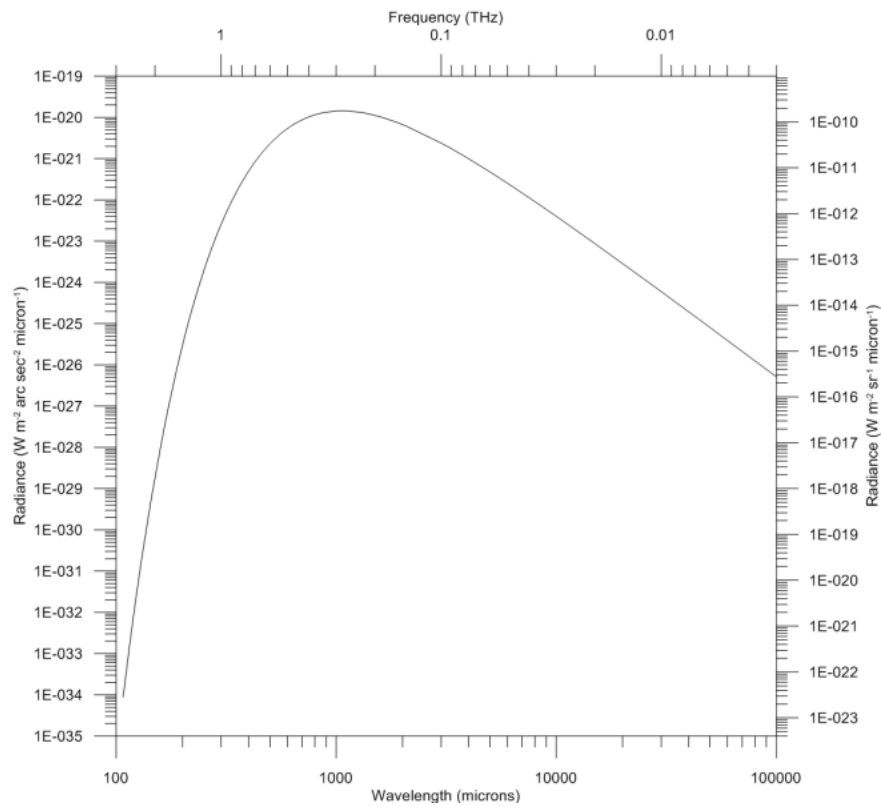


Figure 4.5: The emission of the cosmic microwave background

Analysis on data collected by the Cosmic Background Explorer (COBE) has shown that the CMB is a near-perfect black body at a temperature of 2.726 K (Fixsen 2009). By Wien's Law the intensity peaks at 1.063mm and falls off sharply towards shorter wavelengths as shown in figures 4.4 and 4.5. Therefore, the CMB will not provide significant if any noise in the waveband of this study, but it may need to be considered in far infrared and near millimeter observation missions.

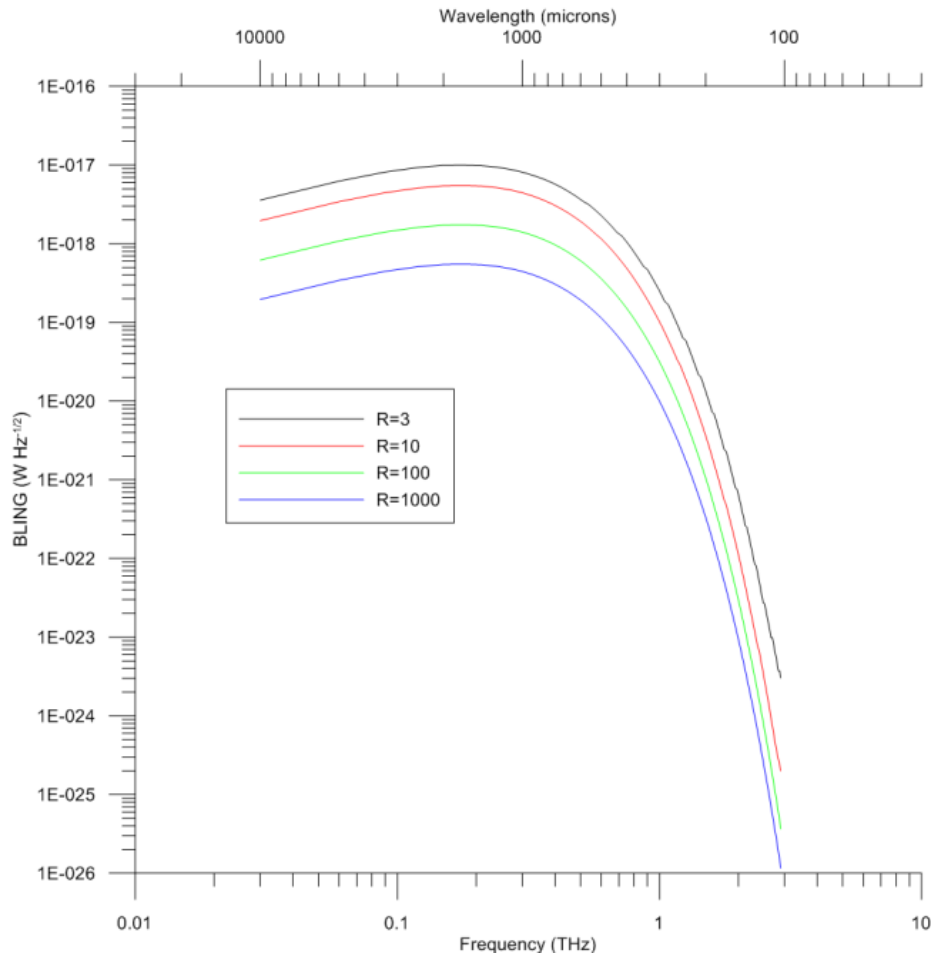


Figure 4.6: BLING generated by the cosmic microwave background

4.3 Cosmic Infrared Background

With the intensity of the cosmic microwave background dropping off at around 100 microns, cosmologists considered the possibility of backgrounds in other wavelength ranges. The cosmic infrared background (CIB) is a general term describing a complex background that has been partially measured from ~ 1 micron to over 500 microns. Theory supporting the CIB first appeared in the 1960s through the work of Partridge and Peebles and has been supported by the measurements from infrared satellites such as COBE and Spitzer in the past few decades (Hauser 2001). The component of the CIB that is relevant to this study is primarily the near-infrared background. The most reliable data in this region was collected in the Cosmic Background Explorer (COBE) mission through collected data between 1 and 240 microns by the DIRBE instrument and out to 1000 microns with the FIRAS instrument though the primary source is with the DIRBE. There exists a split in behavior in the CIB at about 10 microns

(Franceschini et al. 2001). In both cases the background is thought to be largely from light from unresolved galaxies. In other words, the light that we see and name the CIB is actually coming from galaxies that are too far away or faint to be attributed to specific point sources.

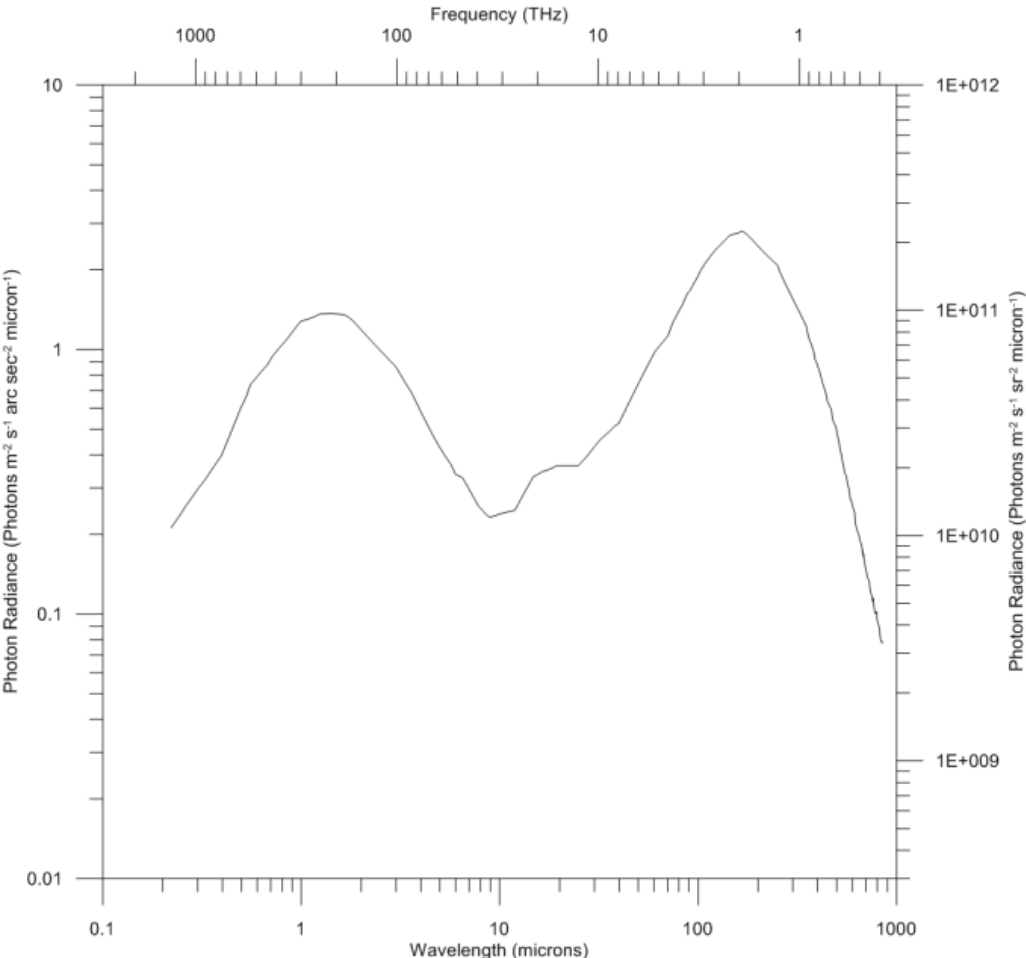


Figure 4.7: The photon emission of the cosmic infrared background.

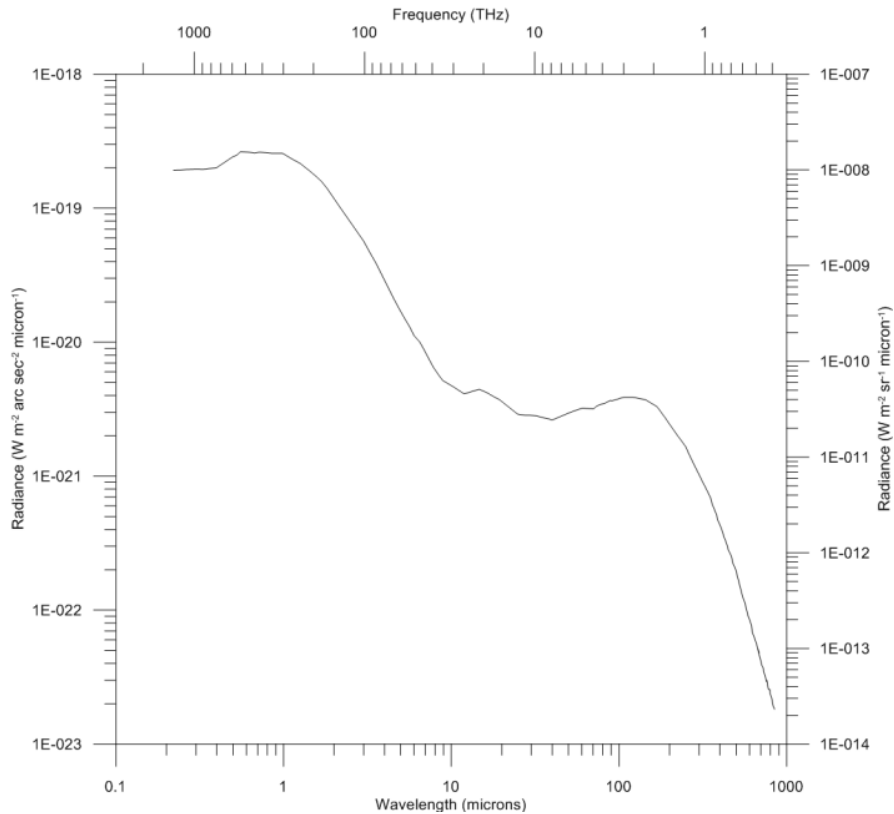


Figure 4.8: The emission of the cosmic infrared background.

For wavelengths less than 10 microns the primary mechanism of photon creation is stellar nucleosynthesis (Franceschini et al. 2006). Stellar nucleosynthesis simply refers to the fusion within a star in which heavier elements are formed. Fusion is a highly exothermal reaction that releases large amounts of energy which is eventually thermalized and ends up as heat in the form of electromagnetic radiation. The majority of the photons released in galaxies that are large enough to show up in the CIB are in the ultraviolet and visible spectrum. However since these galaxies are typically very far away from earth, the light is redshifted towards and often into the infrared.

Beyond 10 microns the infrared background is primarily composed of light from thermal emission of dust particles in a galaxies interstellar medium (ISM). Young, hot stars produce large amounts of light in the ultraviolet some of which is absorbed by the ISM of the star's galaxy. This heats up the dust particles which emit light as grey bodies. Observation by the Infrared Astronomical Satellite (IRAS) in the 1980s helped determine that the primary sources of infrared emission are luminous (LIRGs) and ultra-luminous (ULIRGs) infrared galaxies (Soifer, Neugebauer, and Houck 1987). These galaxies are highly luminous because they have very high star creation rate. For a high star creation rate to be possible there must be a large amount of dust in the galaxy all of which is absorbing energy and emitting in the infrared.

The two regions of the CIB can be seen by the two peaks in Figure 4.7 Since there are only a few windows where the CIB can be directly observed, we use Franceschini’s model to generate a full spectrum.

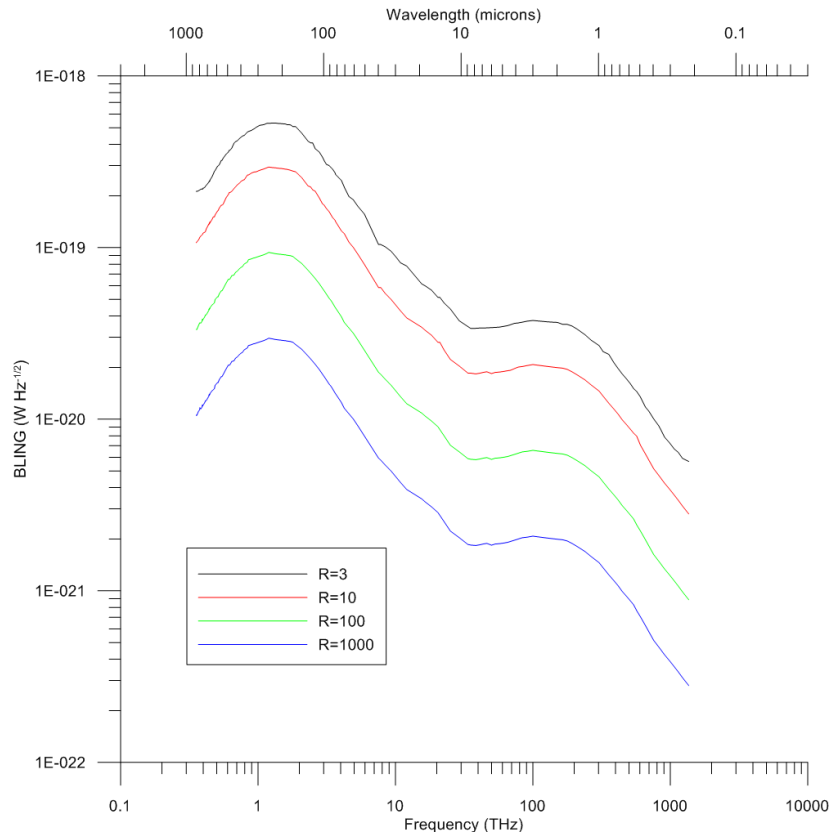


Figure 4.9: BLING generated by the cosmic infrared background

4.4 Zodiacal Emission

The highest intensity extraterrestrial background in the infrared is the emission and reflection of the dust within our solar system. When the COBE Diffuse Infrared Background Experiment (DIRBE) took on the task of resolving the CIB, they were faced with the task of creating precise models of the light emitted within our solar system. We are able to use their models to predict the noise that the zodiacal background will add to our study. To accurately understand the zodiacal background we need to have an understanding of how dust is distributed within our solar system, the manner in which this dust reflects sunlight, and the process in which it absorbs and subsequently re-emits energy from the sun.

To model the zodiacal light we first need a density model of the interplanetary dust (IPD) cloud. The IPD model is the most intensive piece in the full model as it involves creating a spatial model in three dimensions. While the cloud appears to be smooth, there are significant perturbations that need to be taken into account (Reach 1997).

The models of Dr. Bill Reach show that along with a complex spatial structure, the zodiacal background also has variation in its spectral and temporal structures. Plots containing intensities of the zodiacal light

for various directions of view from the earth are shown in Figure 4.7. The high intensity of light emitted combined with the complex structure makes the prospect of a telescope that is sent out of the solar system highly appealing if not currently practical.

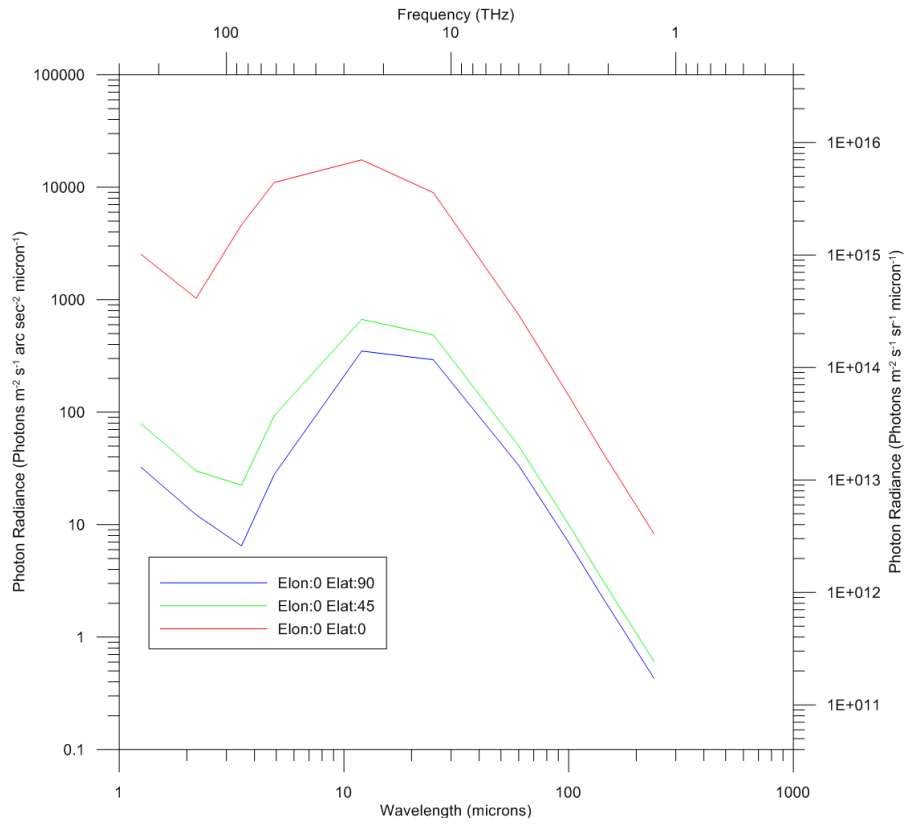


Figure 4.10: The zodiacal background photon emission at three different directions of sight from Earth

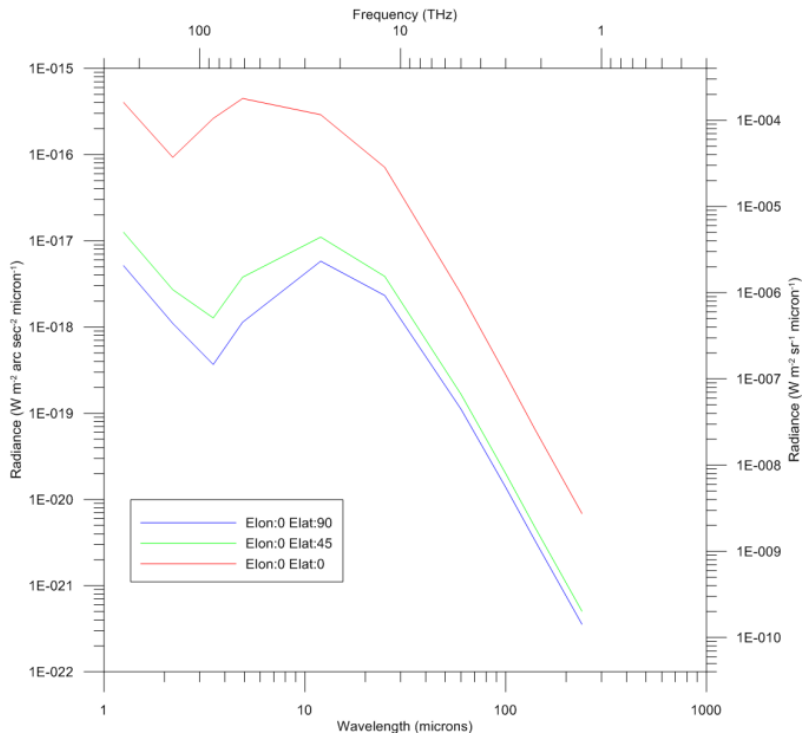


Figure 4.11: The zodiacal background emission at three different directions of sight from Earth

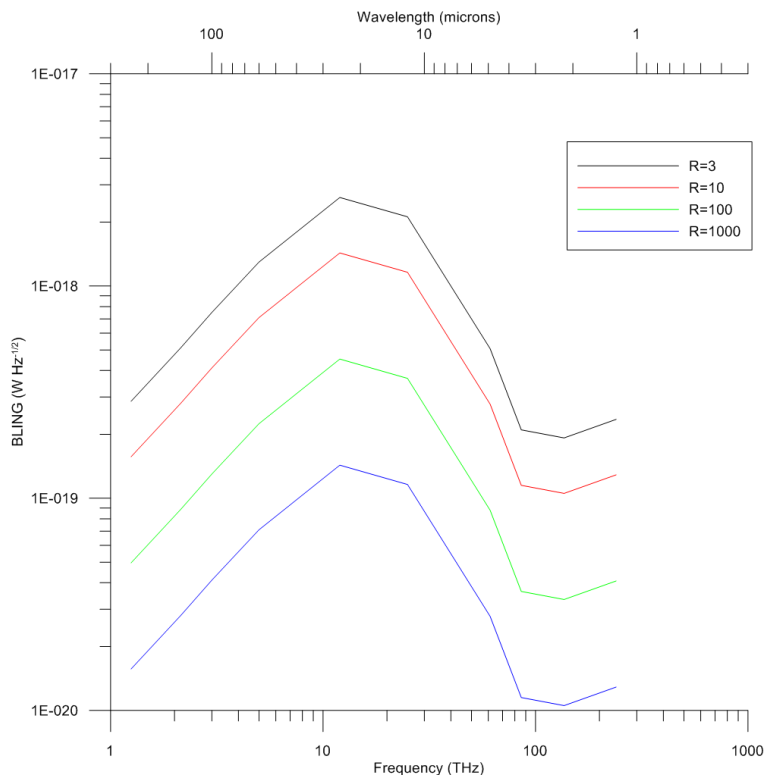


Figure 4.12: BLING generated by the zodiacal background along the GNP 45° zenith

4.5 Other Atmospheric Effects

When considering telescopes located within the Earth's atmosphere we must understand and account for the effect that this large amount of matter has on photons. In this study we examine the radiance or for the amount of noise light generated within the atmosphere. We also must understand and be able to quantify the absorption through a transmission coefficient. Any light passing through the atmosphere will reduce significantly in intensity.

Our atmosphere is primarily comprised of gaseous nitrogen, oxygen, and water vapor as well as numerous trace gases. These gasses absorb energy from the sun and are heated. They then emit radiation just as we say the zodiacal dust radiate. We see these photons as we try to look up through the atmosphere at stars and galaxies and thus must include them in our total noise calculation.

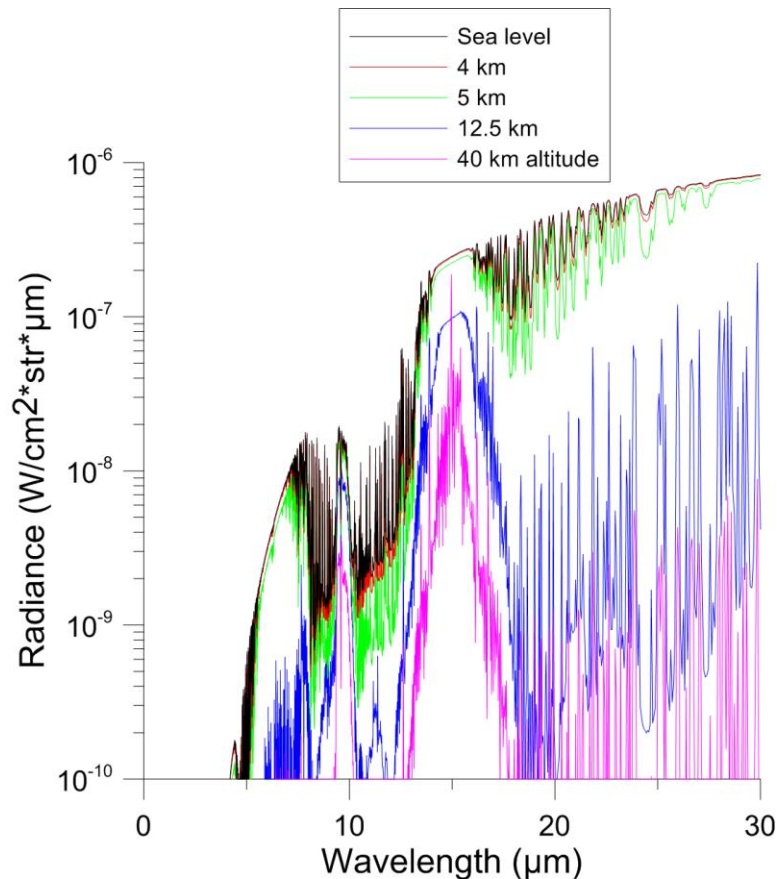


Figure 4.13 The radiance of our atmosphere at various altitudes

Some of the gases in our atmosphere absorb significant amounts of incoming electromagnetic radiation. Ozone is probably the most well-known for its ability to absorb harmful ultraviolet radiation from the Sun. In the infrared water vapor is the primary absorber. Therefore in our experiment it is critical to choose scenarios in which we minimize the amount of water vapor our telescope is looking through. We describe the magnitude of the absorption through the transmission coefficient τ which is a number between 0 and 1 representing the proportion of light that reaches a telescope.

To model these two effects of the atmosphere we turn to the moderate resolution atmospheric transmission model (MODTRAN 5.2). This model allows us to model numerous atmospheric gases, the amount of light they emit, and the transmission they allow. In running our model we chose to have our point of view as a 45° path through the atmosphere. We chose to run the models at altitudes of 0km for sea level, 4km for Mauna Kea and other high altitude ground-based telescopes, 12.5km for the operating altitude of SOFIA, and 40km for the operating altitude of a balloon-based telescope.

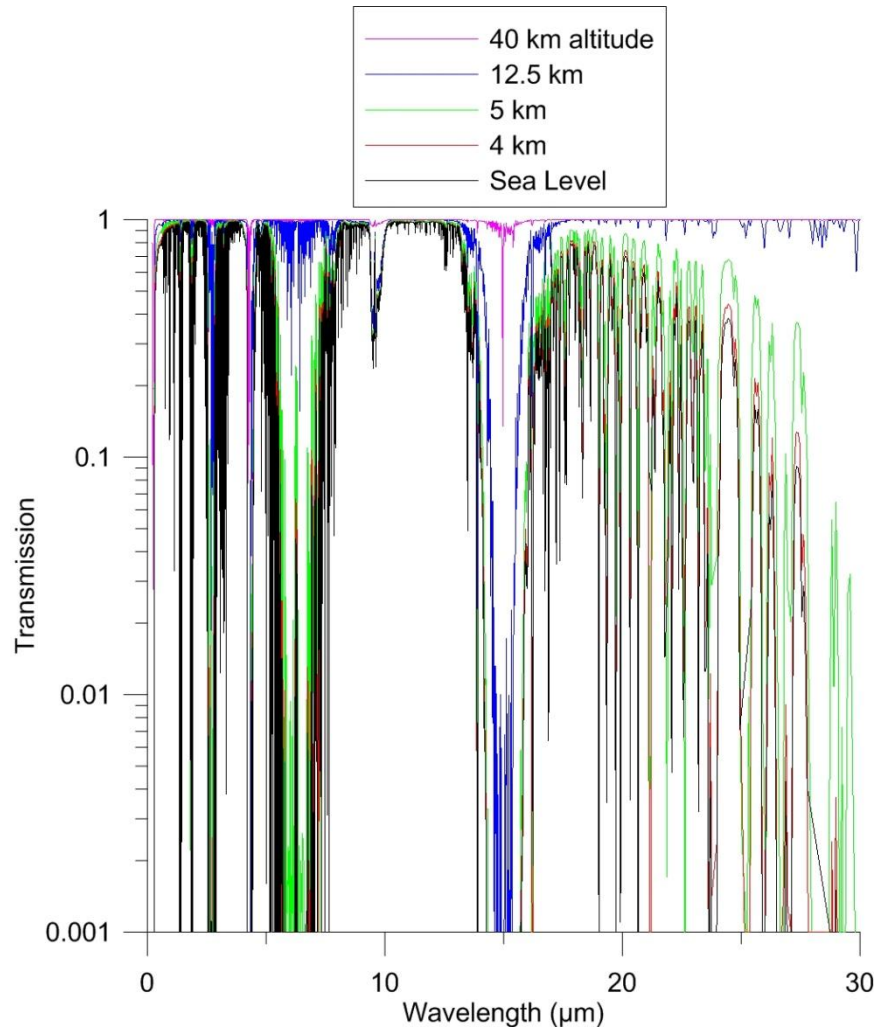


Figure 4.14 The transmission of our atmosphere at various wavelengths.

4.6 Interpolation

Since we are dealing with discrete data we need to have consistent independent vectors between backgrounds. For instance our model of the Zodiacal light has 7 data points whereas our model for the CMB is essentially a continuous function. To enable comparison we fit all of our models onto a new independent axis using linear interpolation. Linear interpolation is a simplistic curve fitting approach that draws straight lines between each data point. We can then approximate intermediate points with our knowledge of these lines.

As a general example assume we know two points (x_1, y_1) and (x_2, y_2) . If we choose a point (x, y) that falls on the line between (x_1, y_1) and (x_2, y_2) the slope of the line from (x_1, y_1) to (x, y) must equal the slope of the line from (x_1, y_1) to (x_2, y_2) as they are along the same line. Therefore we have

$$\frac{y - y_1}{x - x_1} = \frac{y_2 - y_1}{x_2 - x_1} \quad (4.30)$$

From here it is trivial to get an equation for our interpolated y value in terms of a new x value

$$y = y_1 + (y_2 - y_1) \frac{x - x_1}{x_2 - x_1} \quad (4.31)$$

We choose to interpolate all of our data onto a sequence of wavenumbers from 1 to 33,333. A wavenumber describes the frequency of light and has units of cm^{-1} . A wavenumber is a unit of frequency though it is actually the inverse of the wavelength if the wavelength is given in centimeters. Units in terms of wavenumbers are especially useful in integrations as each time the wavenumber is increased by one there is an increase in frequency by about 3.0^{10} Hz or 30 GHz. Uniform bin widths greatly simplify the process of numerical integration.

4.7 Total Noise Calculation

With all of the significant sources of noise quantitatively described we are now prepared to calculate the total noise that a telescope will see at a given location. This comes down to simply summing the BLINGs for each noise source in quadrature

$$BLING_{tot} = \left(\sum_i (BLING_i)^2 \right)^{\frac{1}{2}} \quad (4.32)$$

This is a somewhat incomplete picture as we need to account for the transmission of our atmosphere for noise sources that originate outside of Earth. Thus we must multiply each extraterrestrial BLING by the transmission coefficient for our altitude. We can then write our total BLING as

$$BLING_{tot} = \left(\sum (BLING_{terrestrial})^2 + (\tau \cdot BLING_{cosmic})^2 \right)^{\frac{1}{2}} \quad (4.33)$$

The total BLING is a comprehensive metric for the total noise our system incurs and will be used for the calculation of limiting flux densities as well as integration time when paired with our SED.

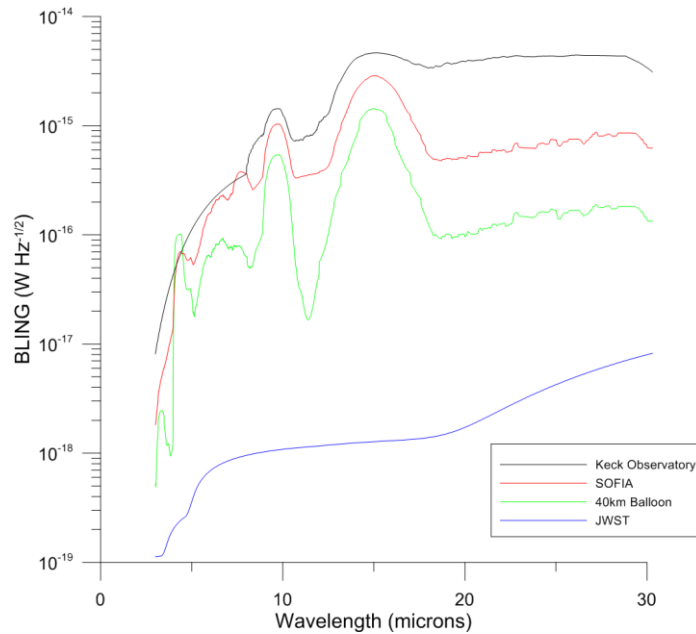


Figure 4.15: The total BLING with $R=10$ for our four idealized telescopes. As mentioned the names associated with these telescopes (Keck, SOFIA) are meant as the equivalent idealized instrument of the same size and at the same site. The “real” Keck and “real” SOFIA are far worse than this primarily due to the fact their actual (“real”) emissivity is far greater than the idealized one we used.

5. Signal

To calculate integration times we need to quantify a signal. For this investigation we will model a galaxy with its Spectral Energy Distribution (SED) or spectral radiance as perceived on Earth. In particular we will use Messier 87 (M87) which is an elliptical galaxy that is close enough to Earth that we do not need to account for the effects of redshift. As in our total noise calculation we will need to determine the effect the Earth’s atmosphere has on light from this galaxy. With the combination of our SED and an absorption function we can integrate over wavelength and receive the total energy, or signal power, which can be used to calculate the integration time. It must be made clear that we proceed with the assumption that M87 is a point source for all of our telescopes. This allows us to compress the entire signal onto one pixel of our detector, which greatly simplifies our calculations. This is a somewhat inaccurate assumption as M87 will not be seen as a point source by any of the telescopes we are modeling. As we proceed with this study we will account for this phenomenon and refine our signal model.

5.1 SED Data

We obtained data on M87 through the NASA/IPAC Extragalactic Database (NED). The database provided a large collection of radiances that had been measured and peer-reviewed over the past fifty years. Figure 5.1 shows the NED generated plot of the data with log radiance plotted against log frequency. As can be seen in figure 5.1, there are frequencies that contain multiple radiance values. To create a signal curve that is easy to analyze we first average these multiple points. The data then must be interpolated

we assumed a volume averaged emissivity function of frequency. A future paper will consider line emission. We model

$$\varepsilon(\nu) \propto \nu^\beta \quad (5.1)$$

The value of β is usually assumed to be between 1 and 2. The spectral energy distribution (SED) of the dust emission can now be expressed as $f(\nu)$

$$f(\nu) \propto \varepsilon(\nu)I(\nu, T)_{bb} \quad (5.2)$$

Where $I(\nu, T)_{bb}$ is the black body radiance with units of $\left[\frac{W}{m^2 Hz sr}\right]$

It is important to note that this model is valid only in the submillimeter to far-IR wavebands. In the mid-IR and near-IR wavebands, dust grains with a temperature greater than T_d and stellar emission will prevent the SED from dropping with a Wien exponential (Blain et al. 2002). In these bands it is instead reasonable to model the SED as a power law

$$f(\nu) \propto \nu^\alpha \quad (5.3)$$

At higher wavelengths, the SED once again deviates from a modified blackbody function. The slope of the SED changes abruptly at about 3 mm, at which the dominant contribution shifts from thermal dust emission to synchrotron radio emission (Blain 1999). Synchrotron radiation is generated by the acceleration of ultra-relativistic charged particles through magnetic fields, and obeys a power law function of frequency

$$f(\nu) \propto \nu^{\alpha_{radio}} \quad (5.4)$$

Where typically $\alpha_{radio} = -0.8$. The SED model we used for all frequencies of concern can now be expressed as a piecewise function

$$f(\nu) \propto \begin{cases} \nu^{\alpha_{radio}}, & \nu < 0.1 \text{ THz} \\ \nu^\beta \left(\frac{2h\nu^3}{c^2}\right) \left(\frac{1}{e^{\frac{h\nu}{k_B T}} - 1}\right), & 0.1 \text{ THz} < \nu < \nu_{midIR} \\ \nu^{\alpha_{high}}, & \nu_{midIR} < \nu \end{cases} \quad (5.5)$$

ν_{midIR} is the transition frequency from the modified blackbody to the high frequency inverse power law. It must be found by fitting data. Additionally, equation 5.5 is only a proportionality; the constants of proportionality can only be found by tailoring the SED to match a particular galaxy with some known values of $f(\nu)$. IRAS data for NGC 958 was fit to yield parameter values $\alpha_{radio} = -0.8$, $\alpha_{high} = -1.95$, $\beta = 2$, and $T_d = 21K$ (Blain et al. 2002, Blain 1999) and shown in figure 5.2.

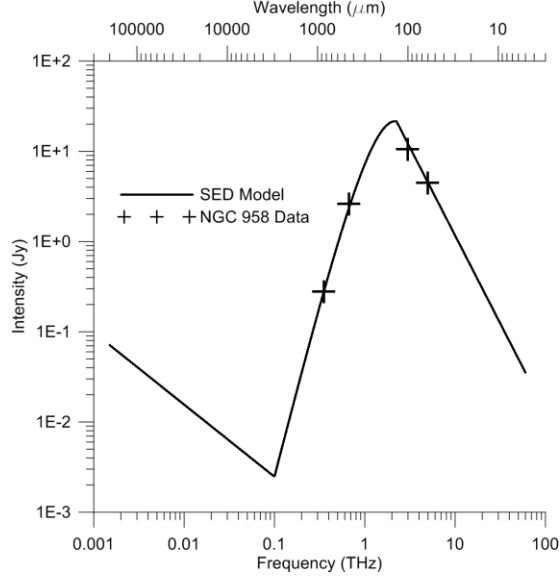


Figure 5.2: Fit piecewise SED model of NGC 958. Parameters: $z = 0.0196$, $T_d = 21\text{K}$, $\alpha_{\text{radio}} = -0.8$, $\beta = 2$, $\alpha_{\text{high}} = -1.95$

NGC 958 has a redshift of 0.0196. In order to model galaxies at different redshifts, the SED must be scaled, which we now describe. The luminosity distance $D(L)$ of an object is defined by the relationship between bolometric (i.e. integrated over all frequencies) flux S and bolometric luminosity L

$$D(L) = \sqrt{\frac{L}{4\pi S}} \quad (5.6)$$

The source function of a galaxy varies widely with frequency, rendering a bolometric approach unhelpful, and differential forms of S and L must be used, $S(\nu)$ and $L(\nu)$. As a result, the k-correction must be applied to either the flux or luminosity because the redshifted object is emitting flux in a different band than in which we are observing.

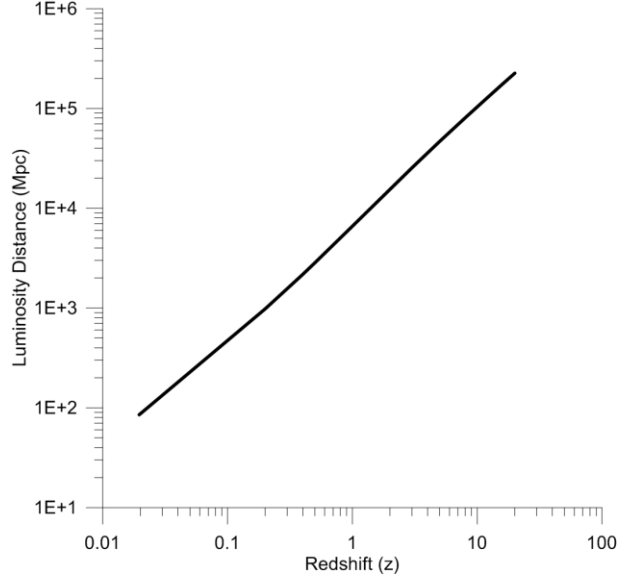


Figure 5.3: Luminosity Distance as a function of redshift for the Benchmark Model of the universe. This is the cosmological model that we assume to generate our SEDs. Parameters assumed: $\Omega_M = 0.3$, $\Omega_L = 0.7$, $w_0 = -1$, $H_0 = 70$

If a source at redshift z emits at frequency ν_{emit} , we observe it at frequency ν_{obs}

$$\nu_{obs} = \frac{\nu_{emit}}{1+z} \quad (5.7)$$

For a bandwidth at the source $\Delta\nu_{emit}$, between frequencies ν_{emit1} and ν_{emit2} , the bandwidth at we observe is $\Delta\nu_{obs}$, between frequencies ν_{obs1} and ν_{obs2}

$$\begin{aligned} \Delta\nu_{emit} &= \nu_{emit2} - \nu_{emit1} = (1+z)\nu_{obs2} - (1+z)\nu_{obs1} \\ \Delta\nu_{obs} &= \frac{\Delta\nu_{emit}}{1+z} \end{aligned} \quad (5.8)$$

The differential flux observed, $S(\nu)$, is related to the differential flux being emitted, L_e , by

$$S(\nu) = \frac{(1+z)L_e}{4\pi D(L)^2} \quad (5.9)$$

In the case of NGC 958, the SED we modeled was not the emitted spectrum, but the spectrum at $z_1 = 0.0196$. As a result, if we want to find the spectrum at some z_2 , we must use equation 5.9 twice and take the ratio of the results

$$\frac{S(\nu_2)}{S(\nu_1)} = \left(\frac{1+z_2}{1+z_1}\right) \left(\frac{D(L_1)}{D(L_2)}\right)^2 \quad (5.10)$$

ν_i is the frequency the observer sees from the galaxy at redshift z_i .

Since we were interested in observing the galaxy at some redshift z_2 , and we know the functional form of $S(\nu_1)$ from equation 5.9, the last step is to map $S(\nu_1)$ into the ν_2 frame (Hogg 1999)

$$\nu_1 = \left(\frac{1+z_2}{1+z_1}\right)\nu_2$$

$$S(\nu_2) = \left(\frac{1+z_2}{1+z_1}\right) \left(\frac{D(L_1)}{D(L_2)}\right)^2 S\left(\left(\frac{1+z_2}{1+z_1}\right)\nu_2\right) \quad (5.11)$$

Equation 5.11 incorporates the effects of the inverse-K correction. Because the absolute change in shifted frequency is proportional to the emitted frequency, the bandwidth of the redshifted signal is narrowed. Because of this compression, the differential flux, $S(\nu)_2$ picks gains an extra factor of $\left(\frac{1+z_2}{1+z_1}\right)$. Additionally, since S_{ν_1} is mapped into the ν_2 frame, if ν_2 is on the Rayleigh-Jeans portion of the SED, then $S(\nu_2)$ will scale as $\sim\left(\frac{1+z_2}{1+z_1}\right)^5$, and will increase significantly for large z .

The inverse K-correction is shown in Figure 5.4 and the correction applied to the template SED is shown in Figure 5.5. The inverse-K correction greatly benefits the observation of millimeter-wave and microwave galaxies with the peak effect at 70 GHz. The effects are less significant in the submillimeter regime, though they do offer benefits at high redshift. Note that the overall effect is to make high redshift galaxies in the far IR much brighter than naively expected from a pure inverse square law analysis. A $z=2$ -equivalent dusty galaxy (if it existed) could be brighter than a $z=1$ dusty galaxy for example. This offers the possibility of a unique probe of high redshift structures.

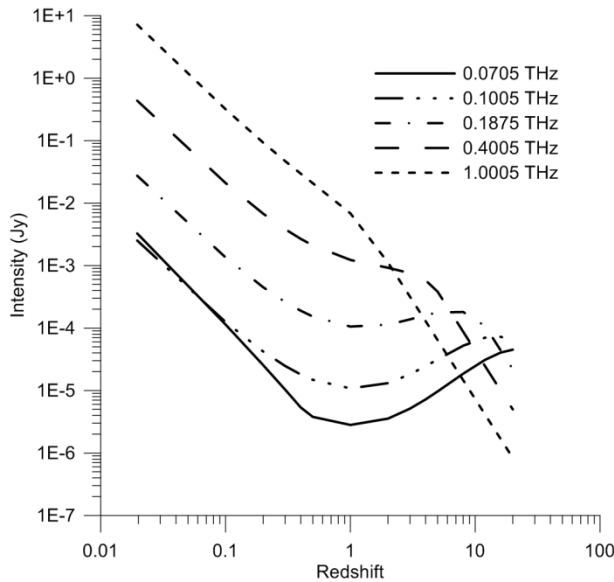


Figure 5.4: Intensity vs. redshift for our model SED highlights the effects of the inverse K-correction for frequencies 0.07-1THz for redshift out to $z=20$.

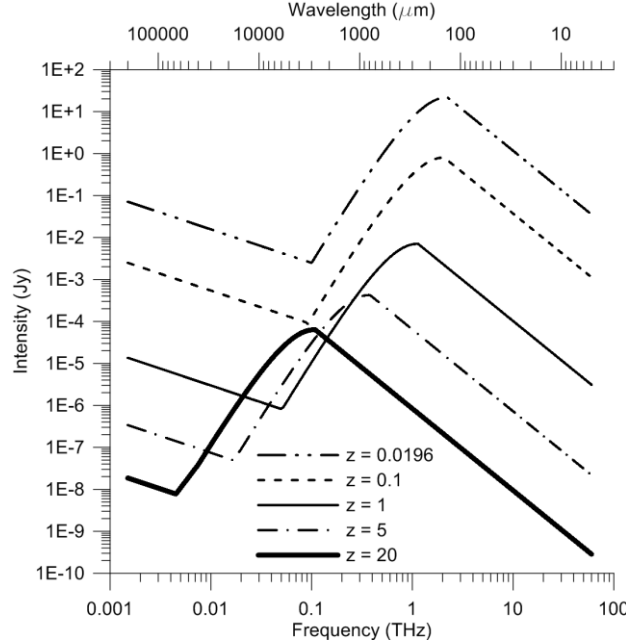


Figure 5.5: Shifted template SED for various redshifts.

5.3 Signal Integration

Similarly to our calculation of BLING we must perform an integration to get the full signal power seen by our detector. By making the assumption that we are viewing a point source we are able to ignore the solid angle component of our radiance and our total signal power can be calculated as

$$P(\nu_0) = \epsilon \pi \left(\frac{d}{2}\right)^2 \int_{\nu_0 - \frac{\Delta\nu}{2}}^{\nu_0 + \frac{\Delta\nu}{2}} \tau(\nu) I(\nu) d\nu \quad (5.12)$$

With d the diameter of the primary mirror, $\tau(\nu)$ the frequency dependent transmission, $\Delta\nu$ the bandwidth, ϵ is the telescope efficiency, and $I(\nu)$ the intensity of the source. Notice that $I(\nu)$ is equivalent to the power per unit bandwidth $S(\nu)$ used in section 4.0.2. The quantity P has units of Watts and can be used in tandem with our total BLING to calculate our integration times. The telescope efficiency ϵ is a number between 0 and 1 that indicates the proportion of the primary mirror area that is able to transmit light to the detector. For this study we assumed that all of our telescopes have efficiencies of 1, but will have to investigate further as we continue to refine our model.

6. Integration Time

We now have the signal for our galaxy as well as a total noise calculation for each of our telescopes. Furthermore the signal and noise are in units that can be manipulated to provide a time in seconds. We specifically wish to find the integration time for our system given a specific signal to noise ratio. The integration time will provide the amount of time our telescope has to point at M87 until it has achieved the desired and statistically significant signal to noise ratio. Integration time is a very good metric for telescope performance because it combines the telescope's ability to pick up the signal as well as the

disadvantages it may encounter due to noise. Furthermore integration time is simple to comprehend and highly relevant to major telescopes in which people sign up for certain amounts of time. If a telescope takes a long amount of time to resolve a simple object, very few scientists will have the ability to work on it.

We must use our values of total BLING and integrated signal to create a signal to noise ratio. By rearranging our definition of BLING we get an expression for our total noise power P_N in Watts

$$\zeta_{tot} = P_N t^{\frac{1}{2}} \Rightarrow P_N = \frac{\zeta_{tot}}{t^{\frac{1}{2}}} \quad (6.1)$$

Now we define our signal to noise ration σ as

$$\sigma = \frac{P_S}{P_N} \quad (6.2)$$

With P_S our total signal power and P_N as above. By combining these two equations and solving for time we have our formula for integration time

$$\sigma = \frac{P_S t^{\frac{1}{2}}}{\zeta_{tot}} \quad (6.3)$$

$$t = \left(\frac{\zeta_{tot} \sigma}{P_S} \right)^2$$

With this simple formula we are now able to calculate and compare integration times across our modeled telescopes. For this study we chose $\sigma=5$ which is typically the smallest signal to noise ratio deemed significant. Figure 6.1 provides us with these integration times for our modeled telescopes. Graphically the integration time is useful as a quick glance at this plot provides a reader with information on the effectiveness of the telescope in units that are easy to comprehend. We now can definitively see the advantages that a space telescope such as James Webb has over a land based telescope such as Keck.

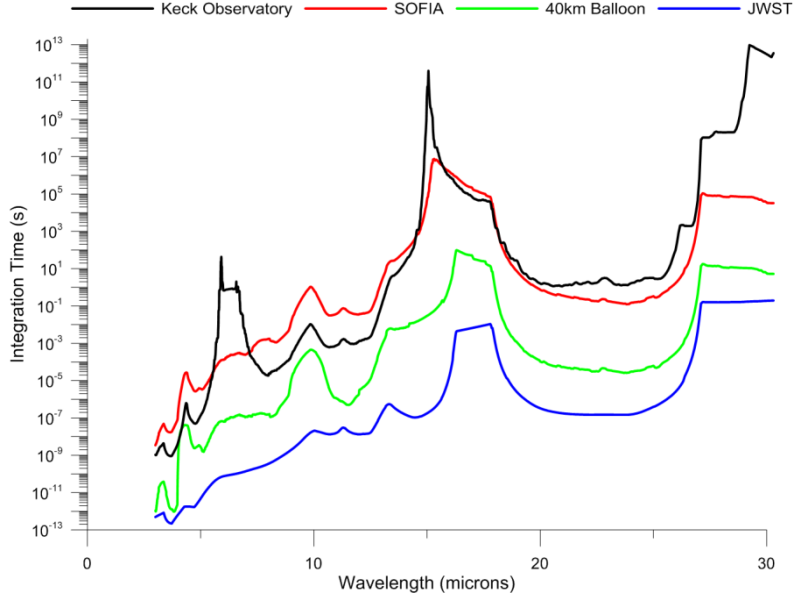


Figure 6.1: Integration times at R=10 for our four telescopes for observing M87 IF it were a point like source (i.e. fits into a single pixel) and SNR of $\sigma=5$.

6.1 Limiting Signal

Another metric used by cosmologists to quantify a telescope's observational power is the limiting flux density. This limiting flux is a signal that is calculated by specifying an integration time and a desired signal to noise ratio. Using these parameters we calculate the minimum signal strength that the telescope can resolve in a given integration time. The mathematical grounds for this calculation are trivial from equation 4.11

$$t = \left(\frac{\zeta_{tot} \sigma}{P_s} \right)^2 \Rightarrow \text{Limiting Signal} = P_s = \frac{\zeta_{tot} \sigma}{\sqrt{t}} [W] \quad (6.4)$$

This calculation only depends on our calculation of total BLING and allows us to check the noise model against recorded data. As can be seen through the comparison of the JWST line in Figure 6.2 our noise model is quite reasonable for JWST and close for SOFIA. We may also calculate our Limiting Flux by “un-integrating” our limiting signal or dividing by the bandwidth

$$\text{Limiting Flux} = \frac{\text{Limiting Signal}}{A * \frac{\nu}{R}} \left[\frac{W}{m^2 Hz} \right] \quad (6.5)$$

Where A is the effective area of the mirror and R is the spectral resolution.

A crucial noise source we have not yet included is the OH emission in the atmosphere which is very high at short wavelengths (1-3 microns). The lack of included OH emission certainly accounts for some of the discrepancy we see between our calculated limiting flux and the recorded value for SOFIA. Also recall that our current model uses a much lower mirror emissivity than has been reported by SOFIA.

Additionally we have not included noise from the detector, which is generally quite small, but will also

bring our model closer to the calculated values. It is also important to note that the true JWST values shown on the left of Figure 6.2 are requirements rather than calculated values. As our calculated values fall consistently and slightly below these requirements, we may have some confidence in our noise model.

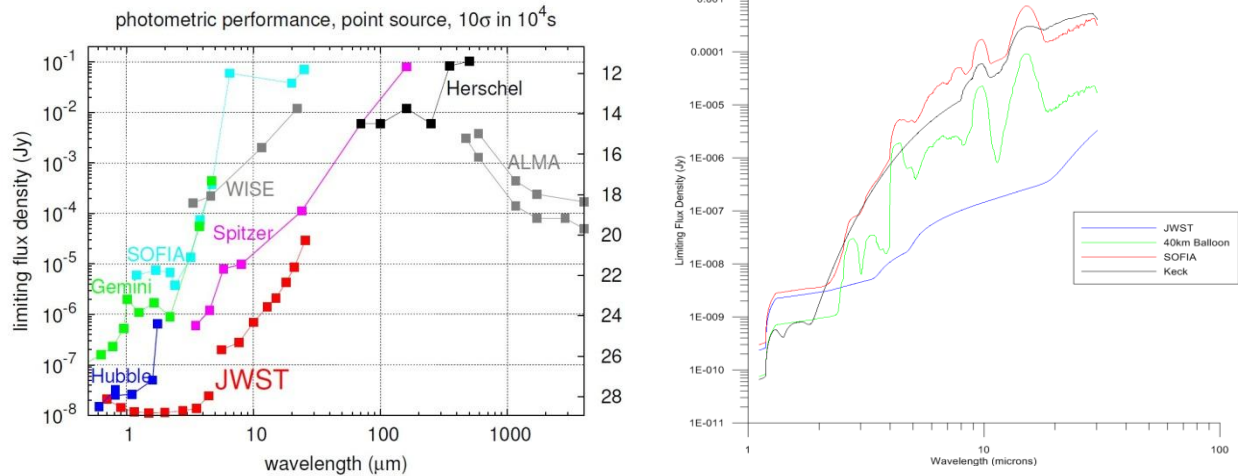


Figure 6.2: Limiting sensitivity plots in Janskys (Jy). Left: A collection of sensitivity values (<http://www.stsci.edu/jwst/science/sensitivity>) Right: Modeled values for our four idealized telescopes. The Keck and SOFIA in reality will be far worse than this.

7. Conclusions

In this study we have made significant progress towards the creation of a comprehensive model for infrared astronomy. We combined models for noise caused by our telescope’s mirror, the Earth’s atmosphere, and extraterrestrial emissions to describe the total noise a telescope will encounter. Furthermore this model can easily be adjusted for different telescope altitudes, mirror coating, and mirror diameter, facilitating comparison between current and hypothetical telescopes. We are able to confirm the accuracy of our noise models through comparison of modeled limited sensitivity with collected data.

To compare our four telescopes in a lifelike situation we used data compiled by the Infrared Processing and Analysis Center (IPAC) for the spectral energy distribution of the Messier 87 galaxy as one example of a source SED. With this signal we calculated integration times for our four telescopes. These integration times provided a simple and clear platform to compare our four telescopes as well as any future simulations. With the infrastructure we have built we can easily expand this study by including more SEDs, such as the dusty SED outlined in section 5.2 as well as more telescope scenarios.

The progress made in this study has merely set the stage for our investigation of near and mid infrared observation. As we proceed, we can improve on our noise model by including the OH emission within the atmosphere as well as the noise generated by the detector of the telescope. We also plan on expanding to more telescope scenarios particularly by modifying the parameters of various more exotic scenarios. Future rounds of simulations will control for particular parameters in our setup, such as

mirror temperature and emissivity. Through such analysis we will be able to pinpoint the most essential features of infrared telescopes.

This study began with investigation of NASA's current super-project James Webb Space Telescope. From early on in our research we knew that JWST was going to be much more sensitive than any current telescope, but we needed a method to quantify this advantage in sensitivity. We now have a model that describes this phenomenon and can progress to determining ideal parameters for infrared telescopes.

8. Acknowledgements

I would like to thank Professor Lubin for working with me since last spring and answering my panicked calls at 2am. Also thanks to the whole UCSB Deepspace group for welcoming me into their lab this summer. Thanks to Professor Higdon for his work as my reader here at the Keck Science Department. A special thank you to Dean Hess and the Dean of Students office at Claremont McKenna College for providing me with the funding I needed to afford my summer of research at UCSB. Last but certainly not least thanks and love to my parents and brothers for supporting me through the past 22 years.

9. References

- Blain, A.W., 1999, MNRAS 309, 4, 955
- Blain, A.W., Smail, I., Ivison, R.J., Kneib, J.-P., Frayer, D.T., 2002, Ph.R., 369, 111
- Bock, J. J., et al., "Emissivity measurements of reflective surfaces at near-millimeter wavelengths" (Applied Optics 34, 1995), pp. 4812-4816
- Cowen, R., "Webb Telescope Delayed, Costs Rise to \$8 Billion." Science. 25 August 2011
<<http://news.sciencemag.org/scienceinsider/2011/08/webb-telescope-delayed-costs.html>>
- Denny, S., Suen, J. Lubin, P. "Fundamental Limits of Detection in the Far Infrared." (2013 Under Review)
- Denny, S. "Limitation on Observing Submillimeter and Far Infrared Galaxies" (2011 UC Santa Barbara Physics)
- Fixsen, D.J., "The Temperature of the Cosmic Microwave Background." (ApJ 707, 2009), pp. 916-920
- Franceschini, A., Rodighiero, G., Vaccari, M., "Extragalactic optical-infrared background radiation, its time evolution and the cosmic photon-photon opacity." (A&A 487, 2008), pp. 837-852
- Gardener, J. P. et al., "The James Webb Space Telescope." (Space Science Reviews, 2006), pp. 485-606
- Goodrich, R. W., "NIRC-2 Observer's Manual." 13 Dec 2002
<<http://www2.keck.hawaii.edu/inst/nirc2/Manual/ObserverManual.html>> Accessed: 25 Nov 2012
- Hauser, M. G., and Dwek, E., "The cosmic infrared background: measurements and implications." (Annual review of A&A 2001)
- Hogg, D. W. 1999 arXiv:astro-ph/9905116
- Lightsey, Paul A., et al., "Optical transmission for the James Webb Space Telescope." (SPIE 2012 under review)
- Lensen, N., et al., "Fundamental Limits of Detection in the Near and Mid Infrared." (2013 in preparation)
- National Research Council. New Worlds, New Horizons in Astronomy and Astrophysics. Washington, DC: The National Academies Press, 2010.
- Planck Collaboration, "ESA Planck Blue Book, Technical Report." (ESA-SCI, 2005)
<<http://arXiv.org/abs/astro-ph/0604069>>
- Reach, W. T., "The structured zodiacal light: IRAS, COBE, and ISO observations." 13 Dec, 2002,
<<http://www2.keck.hawaii.edu/inst/nirc2/Manual/ObserverManual.html>> Accessed: 11 Nov 2012
- Soifer, B. T., et al., "The IRAS view of the Extragalactic Sky." (Annual review of A&A 1987)
- Xu, J., Lange, A.E., Bock, J.J., "Far-Infrared Emissivity Measurements of Reflective Surfaces." Submillimetre and Far-Infrared Space Instrumentation, Proceedings of the 30th ESLAB Symposium (ESTEC, Noordwijk, The Netherlands, 1996), pp. 69-72

“Eddy Current Technology Incorporated: Conductivity of Metals sorted by Resistivity.” Eddy Current Technology. 1984. <<http://www.eddy-current.com/condres.htm>> Accessed: 21 Aug 2012

“Gemini South's Secondary Mirror Sports Shiny Silver Coat.” Gemini Observatory. 2003. <www.gemini.edu/node/103> Accessed: 2 Aug 2012